A Readily Obtained Alternative of 1H-benzo[f]indole towards Room Temperature Ultralong Organic Phosphorescence

Xiaohua Fu,[†,&] Xue Zhang,[†,&] Chen Qian,[†] Zhimin Ma,[‡] Zewei Li,[‡] Hong Jiang[‡] and Zhiyong Ma[*,†]

[†]Beijing Advanced Innovation Center for Soft Matter Science and Engineering, State Key Laboratory of Organic-Inorganic Composites, College of Chemical Engineering, Beijing University of Chemical Technology, Beijing 100029, China.
[‡]College of Engineering, Peking University, Beijing 100871, China.
[&]These authors contributed equally.
[*]Correspondence: mazhy@mail.buct.edu.cn (Zhiyong Ma).

Highlights

- 5H-benzo[b]carbazole performs similarly with 1H-benzo[f]indole in the field of room temperature ultralong oganic phosphorescence via the cation radical-involved mechanism and in some cases behaves better than 1H-benzo[f]indole.
- The synthesis of 5H-benzo[b]carbazole is much easier than 1H-benzo[f]indole, which paves a simple way for the potential applications of RTUOP.
- 5H-benzo[b]carbazole and its derivatives show photo-activated RTUOP in the PMMA film because their corresponding cation radicals are generated by UV irradiation and exhibit aggregation induced red-shift of ultralong phosphorescence at low temperature due to enhanced π-π interactions.

Progress and potential

1H-benzo[f]indole (Bd) is a significant unit in the field of room temperature ultralong organic phosphorescence (RTUOP). However, the synthesis of Bd is rather hard and of low yield, which greatly limits the wide applications of RTUOP. Therefore, exploring readily obtained alternatives of Bd is of great significance and demands to be addressed though it is full of challenges. Herein, 5H-benzo[b]carbazole performs similarly with 1H-benzo[f]indole in the field of room temperature ultralong oganic phosphorescence and in some cases behaves better than 1H-benzo[f]indole. The synthesis of 5H-benzo[b]carbazole is much easier than 1H-benzo[f]indole. 5H-benzo[b]carbazole and its derivatives show photo-activated RTUOP in the PMMA film and exhibit aggregation induced red-shift of ultralong phosphorescence at low temperature. To our best knowledge, this study paves a simple way for the potential applications of RTUOP. Moreover, this work indicates that cation radical-involved mechanism may be universal in the field of RTUOP.

Keywords

5H-benzo[b]carbazole; Red-shifted Ultralong Phosphorescence; Photo-activation; Guest-matrix Doped System; Cation Radical

Graphical abstract

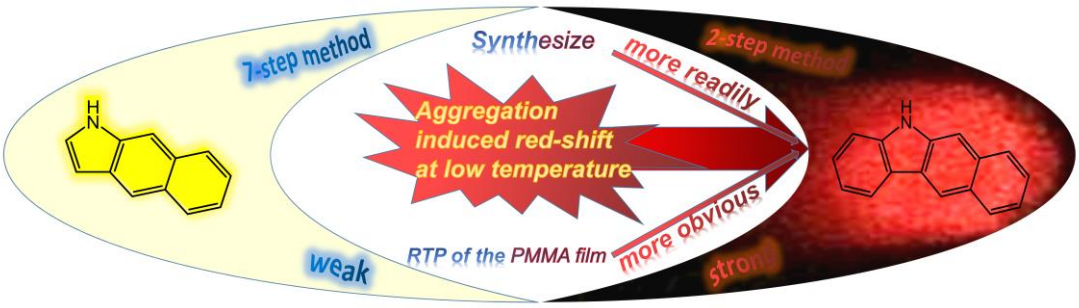

SUMMARY

1H-benzo[f]indole (Bd) is a significant unit in the field of room temperature ultralong organic phosphorescence (RTUOP). However, the synthesis of Bd is rather hard and of low yield, which greatly limits the wide applications of RTUOP. Therefore, exploring readily obtained alternatives of Bd is of great significance and demands to be addressed though it is full of challenges. Herein, we report a new unit named 5H-benzo[b]carbazole (BCz) which can function similarly with 1H-benzo[f]indole (Bd) in RTUOP. BCz can be obtained facilely *via* two steps of reactions while the synthesis of Bd requires seven steps of tedious reactions. Excitingly, readily obtained BCz is an excellent alternative of Bd in RTUOP and shows some advantages in comparison with Bd. Firstly, BCz and its derivatives exhibit distinctive red-shifted red ultralong phosphorescence at 77 K while Bd does not. Secondly, BCz demonstrates remarkable photo-activated yellow ultralong phosphorescence at room temperature while the phosphorescence of Bd is difficult to be activated at room temperature. Thirdly, BCz derivatives (CNPyBCz and CNBrBCz) display similar photo-activated yellow ultralong phosphorescence with Bd derivatives at room temperature but the phosphorescent lifetimes are longer. Fourthly, it is shown that BCz and its derivatives emit yellow RTUOP in the powder matrixes besides their carbazole counterparts. It is revealed that BCz and Bd share the same cation radical-involved phosphorescence mechanism featuring charge separation and charge recombination and the redshift of phosphorescence in the aggregated state arises from the enhanced π-π interactions among BCz units. To our best knowledge, this study paves a simple way for the future applications of RTUOP. Moreover, this work indicates that cation radical-involved mechanism may be universal in the field of RTUOP.

INTRODUCTION

Organic materials with room temperature ultralong phosphorescence have been receiving increasing attention due to the merits of low cost, low toxicity, flexible structural modification[1-3] and facile color tuning,[4-8] and their wide applications in bio-imaging/sensing,[9-12] encryption/anti-counterfeiting[13-17] and organic light-emitting devices,[18-20] etc. Screening the literatures, we can find that guest-matrix systems play a vital role in promoting room temprature ultralong organic phosphorescenece (RTUOP).[21-25] Particularly, the Bd/Cz (1H-benzo[f]indole/carbazole) guest-matrix systems, where Bd derivatives and Cz derivatives function as the guest and the matrix, respectively, have been widely studied in the past several years.[26-29] In our previous work,[29] it is revealed that Bd or its derivatives show (photo-activated) RTUOP in polymers such as PMMA or solid powders such as DMAP and Cz derivatives. These findings will facilitate practical applications of RTUOP. For example, flexible responsive polymer films[30-33] can be easily fabricated when Bd derivatives are doped into polymers and they can be applied in photoprinting. Also, if a biocompatible matrix[34,35] is screened out, the Bd@biocompatible matrix system with RTUOP can be applied in high-contrast bio-imaging after RTUOP nanoparticles are prepared. However, we have to be faced with a cruel fact that the synthesis of Bd is rather hard and of low yield, which greatly limits its wide applications.[29] Therefore, exploring readily obtained alternatives of Bd is of great significance and demands to be addressed though it is full of challenges.

Herein, we report a new unit named 5H-benzo[b]carbazole (BCz) which can function similarly with 1H-benzo[f]indole (Bd) in RTUOP (Figure 1a). BCz can be obtained facilely via two steps of reactions while the synthesis of Bd requires seven steps of tedious reactions. Excitingly, readily obtained BCz is an excellent alternative of Bd in RTUOP and shows some advantages in comparison with Bd. Firstly, BCz and its derivatives exhibit distinctive red-shifted red ultralong phosphorescence at 77 K while Bd does not. Secondly, BCz demonstrates remarkable photo-activated yellow ultralong phosphorescence at room temperature while the phosphores-cence of Bd is difficult to be activated under the same condition. Thirdly, BCz derivatives (CNPyBCz and CNBrBCz) display similar photo-activated yellow ultralong phosphorescence with Bd derivatives at room temperature but the phosphorescent lifetimes are longer. Fourthly, it is shown that BCz and its derivatives emit yellow RTUOP in the powder matrix such as their carbazole counterparts. It is revealed that BCz and Bd share the same cation radical-involved phosphorescence mechanism featuring charge separation and charge recombination and the red shift of phosphorescence in the aggregated state arises from the enhanced π-π interactions among BCz units. To our best knowledge, this study paves a simple way for the potential applications of RTUOP. Moreover, this work indicates that cation radical-involved mechanism may be universal in the field of RTUOP.

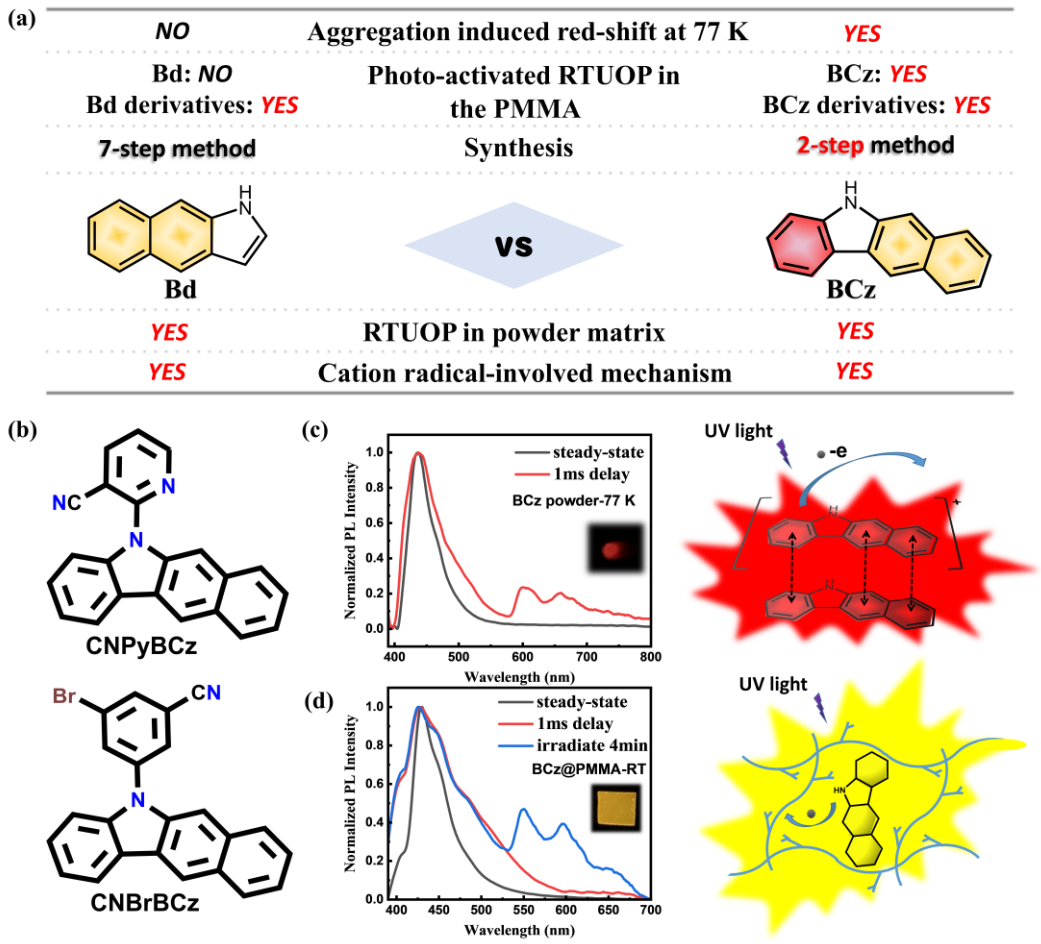

Figure 1. (a) The diagram of superiority of BCz compared to Bd; (b) The molecular structures of BCz derivatives; (c) left: PL spectra of BCz powder at 77 K (Inset: afterglow images for the BCz powder upon the irradiation of light at 365 nm); right: the luminescence mechanism diagram of red-shifted phosphorescence at low temperature; (d) left: steady-state, 1 ms-delayed PL spectra and delayed PL spectra after 4 min irradiation of BCz@PMMA film (1 wt%) at ambient condition (Inset: afterglow images for BCz@PMMA film (1 wt%) upon the irradiation of light at 365 nm); right: the luminescence mechanism diagram of cation radical in the network of PMMA film.

RESULTS AND DISCUSSION

Actually, 5H-benzo[b]carbazole (BCz) contains the fragment of 1H-benzo[f]indole (Bd). Compared with Bd, it is much easier to harvest BCz. BCz can be efficiently gained through two steps of reactions. Firstly, the typical substitution reaction between 1-bromo-2-iodobenzene and naphthalen-2-amine occurred and produced N-(2-bromophenyl)naphthalen-2-amine in a high yield of 82% (Scheme S1). Next, BCz was acquired *via* the intramolecular coupling reaction of N-(2-bromophenyl)naphthalen-2-amine (Scheme S2). Moreover, two donor-acceptor type molecules (CNPyBCz and CNBrBCz) constructed with BCz were synthesized (Scheme S3&Scheme S4) to investigate their properties of RTUOP. Additionally, CNPyCz and CNBrCz were synthesized as the matrixes with the lab-synthesized carbazole (Cz). To fully verify their molecular structures and purity, ^{1}H NMR, ^{13}CNMR, HR-MS and HPLC

were performed. The synthetic procedures and molecular characterization are provided in detail in the Supporting Information (Figure S1-S13).

Photophysical properties in solution

Absorption and photoluminescence spectra of BCz, CNPy-BCz and CNBrBCz were measured in solution (20 μM, Figure S14). The π-π* transitions in THF were located at 212 nm and 270 nm for BCz, 210 nm and 265 nm for CNPyBCz, 209 nm and 270 nm for CNBrBCz, respectively. The n-π* transitions of BCz appeared at 330 nm and 380 nm; and the n-π* transitions of CNPyBCz (315 nm and 370 nm) and CNBrBCz (310 nm and 375 nm) were similar with BCz. In THF, BCz showed two emission bands at 403 nm and 423 nm, assigned to the locally excited (LE) emissions. Both CNPyBCz and CNBrBCz showed obvious solvatochromism, verifying their D-A structure. The shifting emission bands in different solvents were ascribed to the intramolecular charge transfer (ICT) emission. And no luminescent band with a long lifetime was detected at room temperature, suggesting that they are not phosphorescence active in solution at room temperature.

However, at 77 K, BCz, CNPyBCz and CNBrBCz in toluene (20 μM) all showed intense yellow ultralong phosphorescence at ~540 nm, ~590 nm and ~650 nm (Figure S15-S17), implying that BCz is a good RTUOP unit and verifying their nature of monomer emission.

Photophysical properties in the monomer state and the aggregated state

To study the monomer phosphorescence of BCz and its de-rivatives, we doped them into PMMA films with the weight ratio of 1%, separately. At room temperature, all the PMMA films of BCz and its derivatives had a luminescence band at ~425 nm (425 nm for BCz, 440 nm for CNPyBCz and 420 nm for CNBrBCz) with a nanosecond lifetime and a millisecond lifetime (18.5 ns and 7.4 ms for BCz, 11.2 ns and 75.5 ms for CNPyBCz, and 7.1 ns and 13.9 ms for CNBrBCz), suggesting that it contained fluorescence and delayed fluorescence (Figure S27-S29). No ultralong phosphorescence was detected. At 77 K, all the PMMA films displayed intense yellow afterglow and three ultralong phosphorescence bands at ~550 nm, ~600 nm and ~650 nm (almost the same as the phosphorescence bands in the toluene solution at 77 K) with newly emerging second-scale lifetimes (1019.5 ms, 890.4 ms and 794.3 ms for BCz; 1389.7 ms, 1367.4 ms and 1354.7 ms for CNPyBCz; 1036.6 ms, 1017.1 ms and 1000.8 ms for CNBrBCz; Figure S30-S32). The variable temperature photoluminescence (PL) spectra (Figure S33) confirmed that the 425 nm emission band was composed of fluorescence and delayed fluorescence, and the three phosphorescence bands over 545 nm were assigned to ultralong phosphorescence. Thus, BCz and its derivatives function almost the same as Bd and its derivatives in the monomer state but the phosphorescence lifetime of BCz is much longer than that of Bd.

Interestingly, compared with the monomer state, BCz and its derivatives exhibited red-shifted ultralong phosphorescence at 77 K in the aggregated state (Figure 1c and Figure S20), which is totally different from Bd and its derivatives. At room tem-perature, all the original powder samples of BCz, CNPyBCz and CNBrBCz owned an emission band at ~450 nm and similarly this band consisted of two components including fluorescence and

delayed fluorescence due to their two lifetimes (10.7 ns and 7.7 ms for BCz, 9.3 ns and 2.5 ms for CNPyBCz, and 1.2 ns and 13.1 ms for CNBrBCz; Figure S21-S23). No ultralong phosphorescence was detected. At 77 K, all the powders showed red afterglow with three new red-shifted phospho-rescence bands at ~600 nm, ~660 nm and ~730 nm (360.9 ms, 329.6 ms and 290.1 ms for BCz; 1637.9 ms, 627.6 ms and 26.2 ms for CNPyBCz; 174.0 ms and 138.0 ms for CNBrBCz; Figure 2a-2c). In the variable-temperature PL spectra, the intensity of the new emission bands over 600 nm increased significantly along with the decrease of temperature, verifying their characteristics of ultralong phosphorescence (Figure 2d-2f). The red shift of ultralong phosphorescence might arise from enhanced π-π interactions among BCz units with an extended conjugated structure, which was supported by the single-crystal analysis of CNPyBCz (Figure S43&Table S3).

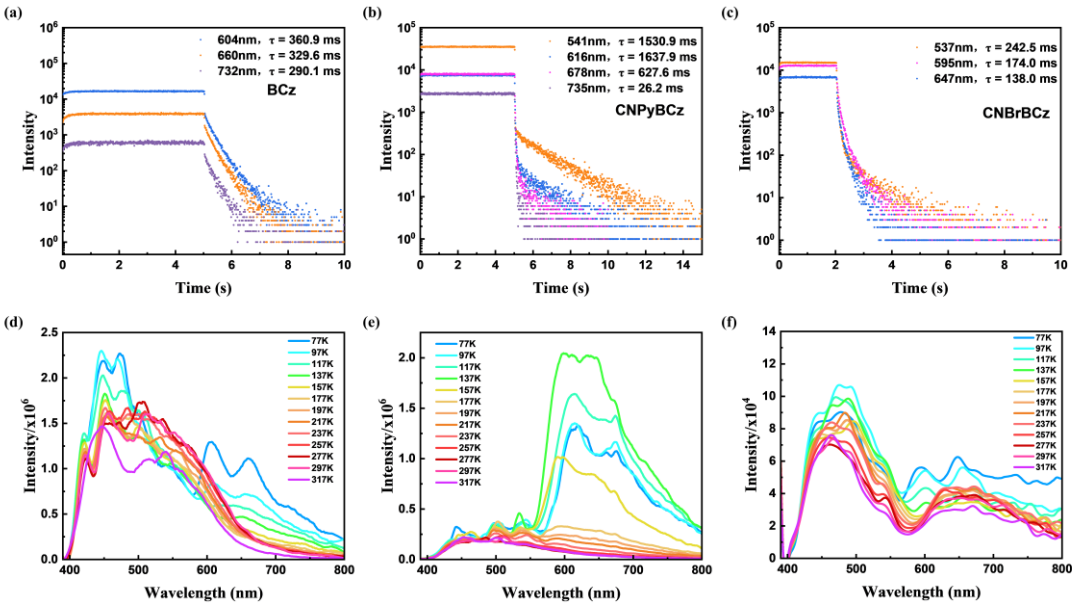

Figure 2. Decay spectra of (a) BCz, (b) CNPyBCz and (c) CNBrBCz powders at 77 K; variable-temperature delayed PL spectra of (d) BCz, (e) CNPyBCz and (f) CNBrBCz powders. (λ_{ex} = 365 nm)

To evidence this assumption, we cultivated the single crystals of BCz and its derivatives. Luckily, we successfully obtained the single crystal of CNPyBCz (Figure S43). In the single crystal, CNPyBCz adopted a twisted geometry with a dihedral angle of 52.71o between BCz and pyridine. CNPyBCz crystallized according to the space group of P 1 21/c 1 (No. 14) belonging to the monoclinic crystal system. Each unit cell contained four molecules. Each BCz unit interacted with the adjacent four molecules via multiple intermolecular interactions of π···π (3.442 Å, 3.289 Å), C-H···π (2.713 Å, 2.713 Å, 2.879 Å), C-H···N (2.458 Å, 2.723 Å). It is rational that these interactions will help lower the energy level of the triplet excitons and lead to the red shift of ultralong phosphorescence.

Photo-activated room-temperature ultralong phosphorescence in the PMMA film

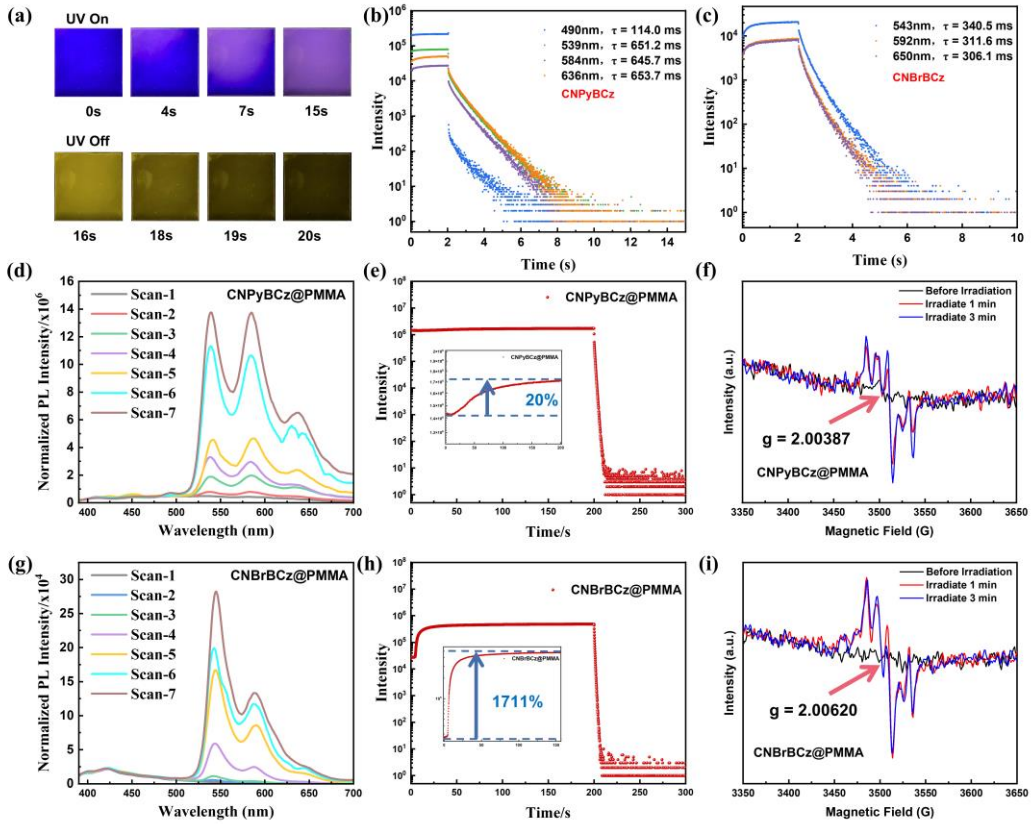

Figure 3. (a) Luminescent images of CNBrBCz@PMMA film (1 wt%) taken at different time points for the whole photo-activated process; decay spectra of (b) CNPyBCz@PMMA film (1 wt%) and (c) CNBrBCz@PMMA film (1 wt%) at ambient condition; the photo-activated phosphorescence enhancement of (d) CNPyBCz and (g) CNBrBCz in the PMMA film monitored by 1 ms-delayed spectra PL spectra at ambient condition; the kinetic scannings of (e) CNPyBCz and (h) CNBrBCz in the PMMA film at ambient condition (Insert: the intensity increase of the CNPyBCz and CNBrBCz films during the kinetic scanning); ESR spectra of the (f) CNPyBCz and (i) CNBrBCz films before irradiation and after irradiation at ambient condition. (λ_{ex} = 365 nm)

Surprisingly, BCz, CNPyBCz and CNBrBCz all demonstrated photo-activated ultralong phosphorescence in the PMMA film at room temperature. As mentioned above, the PMMA films of the three molecules all showed no room temperature ultralong phosphorescence band in the delayed PL spectra before photo activation. However, for BCz (Figure 1d&Figure S27), after 4 min irradiation under 365 nm UV light, yellow afterglow newly emerged and three new emission bands appeared at 550 nm (τ=400.8 ms), 600 nm (τ=418.0 ms) and 650 nm, which have been proved as ultralong phosphorescence. Similarly, for CNPyBCz, its PMMA film showed yellow afterglow and three new ultralong phosphorescence bands at ~550 nm (τ=651.2 ms), ~600 nm (τ=645.7 ms) and ~650 nm (τ=653.7 ms) after UV irradiation (Figure 3b&Figure S28). Particularly, comparing photo-activated room-temperature ultralong phosphorescence of the three

molecules, CNBrBCz is much better than BCz and CNPyBCz, probably owing to the heavy-atom effect of bromine. The images of the photo-activated process of CNBrBCz were recorded with the portable UV light (365 nm) as the irradiation source (Figure 3a). The original PMMA film was deep blue. The photo-activation started at the time point of 4s and ended at 15 s. Once removing the UV light, intense yellow ultralong phosphorescence could be observed by naked eye. The photo-irradiated PMMA film of CNBrBCz gave the strongest yellow afterglow with the ultralong phosphorescence bands at ~543 nm (τ=340.5 ms), ~592 nm (τ=311.6 ms) and ~650 nm (τ=306.1 ms) (Figure 3c).

To carefully monitor the photo-activated enhancement of ul-tralong phosphorescence, in-situ delayed PL spectra and kinet-ic scanning were conducted. We fixed the PMMA films on the sample stage of FLS980 fluorescence spectrophotometer and performedcontinuous repetitive scannings. Increasing the scanning number means prolonging the photo-activation time. For CNPyBCz, the in-situ delayed PL spectra showed that the three phosphorescence bands were almost undetectable at the first scanning and intensity of the three ultralong phosphores-cence bands enhanced significantly accompanied with the increasing scanning number (Figure 3d), verifying its unique property of photo-activated room-temperature ultralong phosphorescence. CNBrBCz exhibited the similar photo-activated in-situ delayed PL spectra with CNPyBCz but the phosphorescence intensity increment of CNBrBCz was much larger than that of CNPyBCz (Figure 3g), confirming the heavy atom effect of bromine. Furthermore, the kinetic scanning (Figure 3e&3h) revealed that the photo-activated process of CNPyBCz and CNBrBCz last 200 s and 150 s, respectively; and the phosphorescence intensity at 600 nm increased by 20% and 1711% for CNPyBCz and CNBrBCz after photo-activation, respectively.

Our previous work discloses that ultralong phosphorescence of Bd originates from its cation radicals.[27,29] It is rational that BCz and Bd share the similar phosphorescence mechanism because of their similar phosphorescence properties. To illuminate the photo-activated mechanism of ultralong phospho-rescence of BCz (derivatives), electronic spin resonance (ESR) measurement was subjected to their PMMA films. For BCz (Figure S34), its original PMMA film showed no ESR signal before UV irradiation, suggesting that there are no radicals at this state. After UV irradiation for 2 min, an ESR signal ranging from 3450 G to 3550 G emerged obviously, indicating that cation radicals of BCz are generated by photo activation. Moreover, quantity of the cation radicals accumulated when UV irradiation extended to 5 min, which was reflected in the continuous increase of the ESR signal. The g value of the cation radical of BCz was calculated to be 2.00351 and was close to the g value of a free electron. As for CNPyBCz and CNBrBCz (Figure 3f&3i), similarly, ESR signal was undetectable before UV irradiation and newly appeared after 1 min UV irradiation. Different from BCz, intensity of the ESR signal after 3 min irradiation was kept almost unchanged compared with 1 min irradiation, revealing that it is more rapid to activate CNPyBCz and CNBrBCz than BCz. It is found that BCz shows low compatibility with PMMA due to its large conjugated structure and easily aggregates in the PMMA film, which limits the photo-activation rate of BCz. The g

values were calculated to be 2.00387 and 200620, respectively and also approached to the g value of a free electron. Therefore, cation radicals play a key role in the photo-activated room temperature ultralong phosphorescence in the system of BCz.

Doping BCz derivatives into powder matrixes

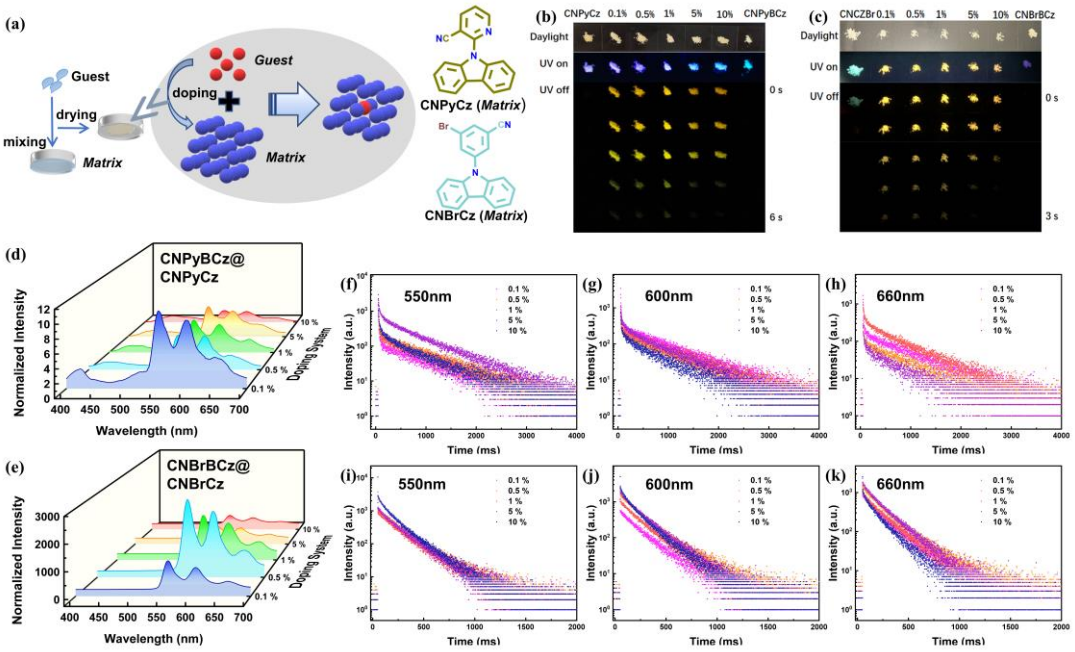

Figure 4. (a) The doping scheme of BCz derivatives as guests into matrix (CNPyBCz@CNPyCz and CNBrBCz@CNBrCz); lumines-cent and phosphorescent images at different dopant ratios for the doped systems of (b) CNPyBCz@CNPyCz and (c) CNBrBCz@CNBrCz; delayed PL spectra of (d) CNPyBCz@CNPyCz and (e) CNBrBCz@CNBrCz at ambient condition; decay spec-tra at 550 nm, 600 nm and 660 nm of (f-h) CNPyBCz@CNPyCz and (i-k) CNBrBCz@CNBrCz with different ratios at ambient con-dition. (λ_{ex} = 365 nm)

As documented,[26,28,36-38] trace amount of Bd enables carbazole derivatives with intense yellow room temperature ultralong phosphorescence. Among the reported Cz-based organic phosphorescence systems,[39-42] in fact, Bd (derivatives) and Cz (derivatives) function as phosphorescence units and matrixes, respectively. Amazingly, we fabricated a new RTUOP guest-matrix system where CNPyBCz (or CNBrBCz) and its counterpart of carbazole CNPyCz (or CNBrCz) function as guest and matrix (Figure 4a), respectively. As expected, pure powders of CNPyCz and CNBrBCz synthesized from lab-prepared Cz do not show any yellow ultralong phosphorescence at room temperature (Figure S40). For CNPyBCz, it was doped into the matrix CNPyCz with the weight ratio ranging from 0%~10%. In Figure 4b, all the doped powders remained blue emitting under the 365 nm light, suggesting that (delayed) fluorescence was still dominant, which was confirmed by the PL spectra (Figure S35). Once the UV light was turned off, intense yellow afterglow could be observed by naked eye (Figure 4b), confirming that this guest-matrix system is highly active in RTUOP. The steady-state and delayed PL spectra showed that the doped powder with 0.1% weight ratio emitted the strongest yellow afterglow (Figure 4d) and the

lifetimes of the three ultralong phosphorescence bands at 550 nm, 600 nm and 650 nm were tested to be 817.2 ms, 803.5 ms and 780.4 ms (Figure 4f-4h&Table S1). When the dopant weight ratio increased over 0.1% gradually, intensity of ultralong phosphorescence weakened significantly due to the quenching effect but the lifetimes changed slightly from ~800 ms to ~600 ms.

Also, CNBrBCz was doped into the matrix CNBrCz and the doping ratio changed from 0% to 10%. Different from CNPyBCz, the pure powders of CNBrBCz and CNBrCz were both blue emissive but all the doped powders were yellow emitting under the 365 nm light (Figure 4c), indicating that yellow ultralong phosphorescence was dominant. Indeed, intensity of the ultralong phosphorescence bands over 550 nm was much higher than that of the fluorescence bands (at ~450 nm) (Figure 4e&Figure S36). Similarly, intense yellow afterglow appeared when UV light was off (Figure 4c) and CNBrBCz@CNBrCz was also an excellent RTUOP guest-matrix system. The steady-state and delayed PL spectra showed the optimal doping ratio was 0.5% (Figure 4e) and the lifetimes of the three ultralong phosphorescence bands at 550 nm, 600 nm and 650 nm were calculated to be 199. 9 ms, 203.6 ms and 201.9 ms (Figure 4i-4k&Table S2). Comparing CNBrBCz with CNPyBCz, it is revealed that the heavy atom effect of bromine strengthens the ultralong phosphorescence of the CNBrBCz@CNBrCz doping system but shortens its lifetime by promoting intersystem crossing (ISC), agreeing well with previous work.[29,43-45]

To elucidate the phosphorescence mechanism of the above guest-matrix system, ESR measurement was carried out. As comparison, for the pure powders of CNPyCz and CNBrCz (as matrix), almost no ESR signal was detected, verifying that radi-cal cations don’t exist in the pure matrix powder. Remarkably, the ESR signal ranging from 3450 G to 3550 G enhanced sig-nificantly at room temperature for the CNPyBCz@CNPyCz and CNBrBCz@CNBrCz doped powders (1 wt% and 5 wt%), confirming that the radical cations of CNPyBCz (CNBrBCz) can be stabilized by its corresponding matrix CNPyCz (CNBrCz) (Figure S42g-S42j). Furthermore, the pure powders of BCz, CNPyBCz and CNBrBCz showed negligible ESR signal at room temperature (Figure S42a-S42c), in agreement with the fact that all the three pure powders are not phosphorescence active at room temperature. Interestingly, the pure powders of BCz, CNPyBCz and CNBrBCz showed detectable ESR signal at 77 K (Figure S42d-S42f), suggesting that the red-shifted ultralong phosphorescence at low temperature also originates from the radical cations. Furthermore, TD-DFT results support the cation radical-involved phosphorescence mechanism (Table S4-S10&Figure S44-S49).

In addition, besides the carbazole-based matrix, it is found that BBP, DMAP and DBT can also function as effective ma-trixes for BCz derivatives at room temperature (Figure 5&Figure S37-S39). When CNPyBCz or CNBrBCz was doped into the above three matrixes respectively, the characteristic ultralong phosphorescence bands at 550 nm, 600 nm, 650 nm were still kept (Figure S37-S39), indicating that the cation radicals of BCz derivatives can also be stabilized by these matrixes at room temperature. However, the lifetimes of the ultralong phosphorescence bands can be tuned in a large range within

different matrixes. For CNPyBCz, the lifetimes of the 550 nm band in different matrixes were tested to be 91.3 ms (BBP), 449.9 ms (DMAP), 34.8 ms (DBT) (Figure S37-S39). For CNBrBCz, the lifetimes of the 550 nm band in different matrixes were tested to be 57.7 ms (BBP), 467.0 ms (DMAP), 446.8 ms (DBT). Moreover, intensity of the ultralong phosphorescence can be regulated by varying the matrix. When the doping ratio was 1%, the best matrix for CNPyBCz and CNBrBCz was DMAP and DBT, respectively. According to the latest report of Prof. Bin Liu, the structural similarity makes a big difference to the phosphorescence intensity of the guest-matrix systems.[6c] We inferred that the more twisted geometry of CNPyBCz was detrimental to the close interactions between CNPyBCz and DBT, leading to the low phosphorescence intensity. On the contrary, strong interactions may form between CNBrBCz and DBT due to the higher structural similarity and result in the intense afterglow.

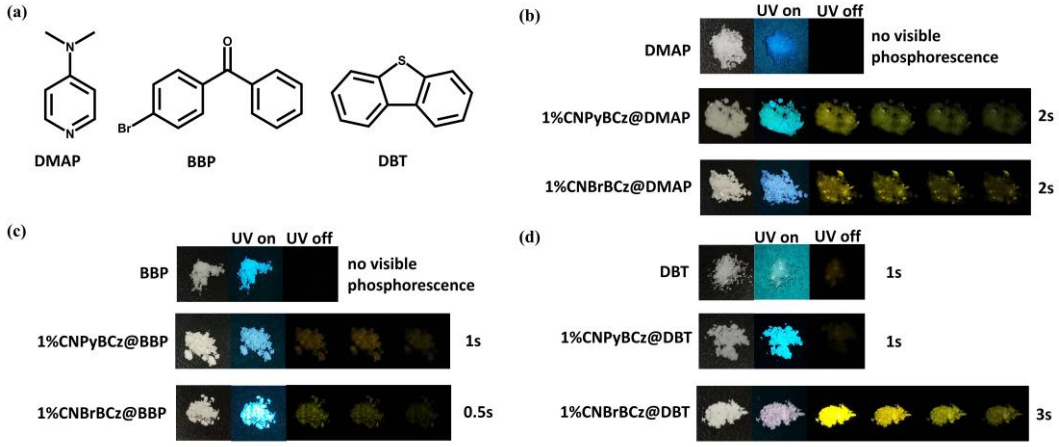

Figure 5. (a) The molecular structures of several new matrixes DMAP, BBP, DBT ; luminescent images of CNPyBCz and CNBrBCz as guests doped into (b) DMAP, (c) BBP, and (d) DBT with the ratio (Guest : Matrix) of 1 wt.% at ambient condition. (λ_{ex} = 365 nm)

TD-DFT calculations and proposed ultralong phosphorescence mechanism

To gain deep insight into the ultralong phosphorescence mechanism of BCz and its derivatives, time-dependent density functional theory (TD-DFT) calculations were performed (Table S4-S10&Figure S44-S49). The calculated energy levels of lowest singlet excited state (S_1) and lowest triplet excited state (T_1) were 3.1563 eV and 2.0095 eV for BCz, 2.5632 eV and 2.0673 eV for CNPyBCz, 3.0100 eV and 2.0456 eV for CNBrBCz (Table S6), respectively. The spin-orbit coupling (SOC) values of S_1/T_1 were calcualted to be 0.51703 cm^{-1} for BCz, 0.46611 cm^{-1} for CNPyBCz, 9.52166 cm^{-1} for CNBrBCz, respectively. It is clear that the SOC values of CNBrBCz are much higher than those of BCz and CNPyBCz (Table S7), verifying the heavy atom effect of bromie. Electron cloud of highest occupied molecular orbital (HOMO) and lowest unoccupied molecular orbital (LUMO) of CNPyBCz and CNBrBCz, and electron cloud of HOMO and SUMO of their cation radicals were carefully analysed. HOMO of CNPyBCz and CNBrBCz was distributed on BCz unit while their LUMOs were dispersed on CNPy unit and CNBr unit (Figure S48&S49), respectively, showing typical donor-acceptor sturcture. However,

when CNPyBCz and CNBrBCz turned into cation radicals (CNPyBCz•+ and CNBrBCz•+), the dihedral angle between BCz unit and the acceptor increased significantly from 66.48°/73.17° to 75.20°/81.40°, leading to a more twisted geometry. Thus, both HOMO and SUMO of CNPyBCz•+ and CNBrBCz•+ were located on the BCz unit (Figure S48&S49), suggesting that the ultralong phosphorescence arose from the LE emission of BCz•+, which agreed well with the experimental results.

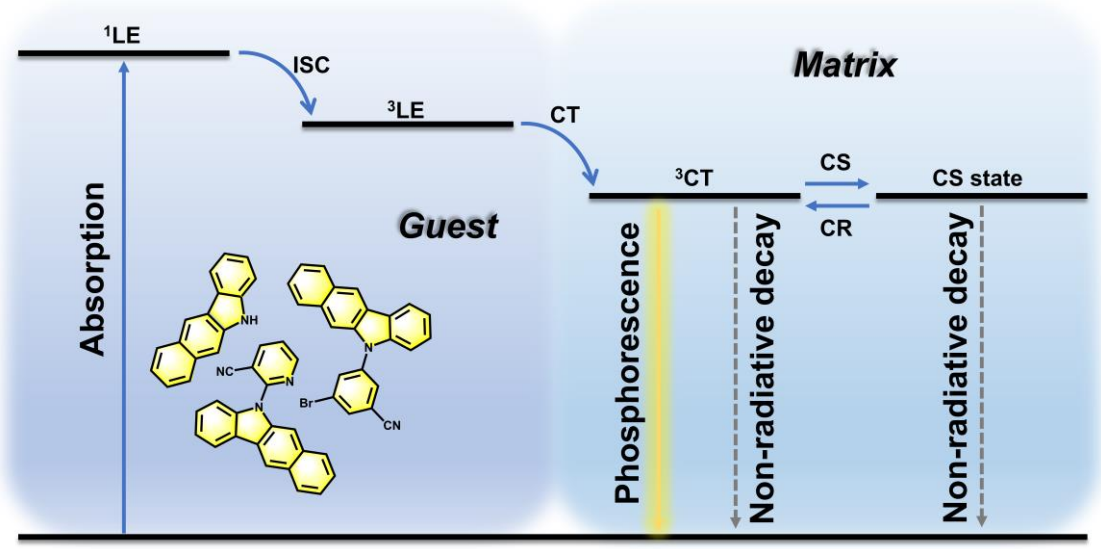

Figure 6. Proposed energy transfer processes of RTUOP. (LE: locally excited state; CT: charge transfer; CS: charge-separated; CR: charge recombination; ISC: intersystem crossing)

On the basis of all the data and the previous work,[46-49] we proposed a cation radical-involved ultralong phosphorescence mechanism (Figure 6) featuring charge separation and charge recombination for the guest-matrix doped systems of BCz and its derivatives. The dynamics of ultralong phosphorescence included five stages. At stage 1, the guest absorbed UV light and was excited to the locally excited singlet state (^{1}LE). At state 2, the ^{1}LE exciton transferred to the locally excited triplet state (^{3}LE) of the guest by intersystem crossing (ISC). At stage 3, charge transfer occurred from ^{3}LE state of the guest to the matrix, and charge transfer triplet excited state (^{3}CT) formed. At stage 4, the ^{3}CT exciton could be trapped and stabilized by charge separation. Cation radicals of the guest and anion radicals of the matrix coexisted and formed charge separation state. Finally, through charge recombination, the charge separation state returned to the ^{3}CT state further to the ground state, emitting ultralong phosphorescence.

Application demonstration

The excellent photo-activated ultralong phosphorescence of BCz derivatives can be applied in lithography, encryption and anti-counterfeiting. Due to the well reversibility of the photo-activated ultralong phosphorescence, different patterns can be printed on the same PMMA film of CNBrBCz with different masks (Figure 7a&7b). The printed PMMA film can recover to the original state at room temperature automatically and heating can

accelerate the recovering process. Excitingly, owing to the long lifetime of the yellow afterglow, high-resolution QR code can be printed on the PMMA film of CNBrBCz (Figure 7c&7d). The printed QR code can be successfully read by the cellphone.

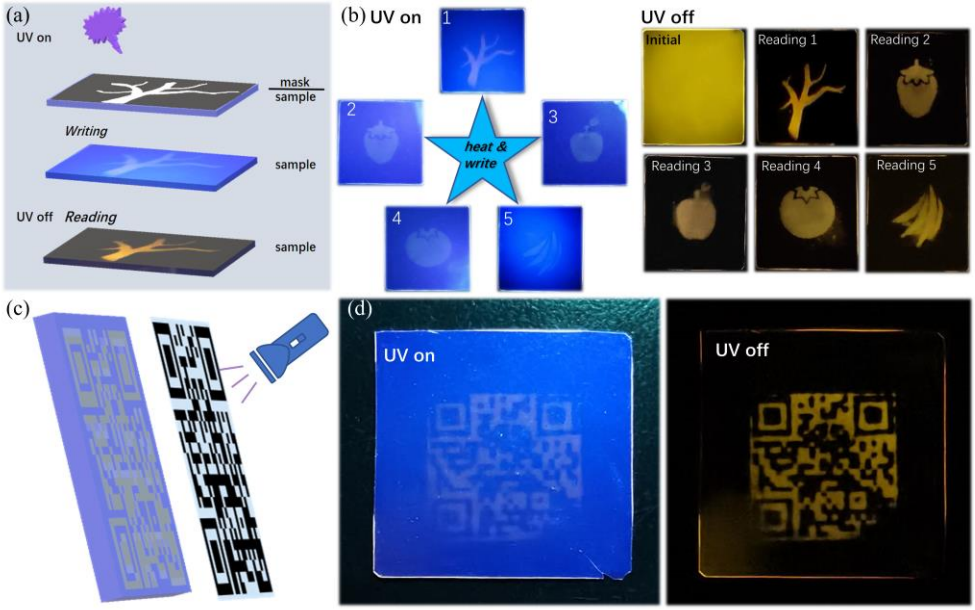

Figure 7. The diagram of applications of the photo-activated CNBrBCz@PMMA films. (a, b) Ink-free printing: reproduce photo-graphs of different patterns multiple times by irradiating under the UV light and heating, and Information encryption: store and write information under UV irradiation and read information after removing the UV light; (c, d) high resolution photolithographic patterning of QR code on the CNBrBCz@PMMA film with fast writing and time-dependent self-erasing properties. (λ_{ex} = 365 nm)

Conclusion

In summary, we successfully discover a readily obtained organic unit 5H-benzo[b]carbazole (BCz) with excellent property of room temperature ultralong phosphorescence. CNPyBCz and CNBrBCz were synthesized and investigated as representatives of BCz derivatives. At low temperature, BCz and its derivatives exhibit yellow ultralong phosphorescence at 550 nm, 600 nm and 650 nm in the monomer state while their ultralong phosphorescence red shifts to 600 nm, 660 nm and 730 nm in their aggregated state, which has never been observed before. The red-shifted ultralong phosphorescence in the aggregated state may arise from the enhanced π-π interactions among BCz units with an extended conjugated structure. Excitingly, the PMMA films of BCz (derivatives) demonstrate photo-activated yellow ultralong phosphorescence at room temperature, due to the photo-promoted generation of cation radials. Moreover, an excellent RTUOP guest-matrix system is established with BCz derivatives and their counterparts of carbazole. When CNPyBCz (CNBrBCz) was doped into CNPyCz (CNBrCz), the mixed powder displayed intense yellow room temperature ultralong phosphorescence because the cation radicals of CNPyBCz (CNBrBCz) can be well stabilized by the Cz-based matrix. Additionally, other matrixes such as DMAP, BBP and DBT can also activate the yellow ultralong phosphorescence of BCz (derivatives) at room

temperature. As CNPyBCz and CNBrBCz were selected randomly in this study, various donor-acceptor structures constructed with BCz can be designed to optimize the property of ultralong phosphorescence, which may open a new research direction in organic phosphorescence.

EXPERIMENTAL PROCEDURES

Full experimental procedures are provided in section S2 of Supplemental Information.

Resource Availability

Lead Contact

Further information and requests for resources and materials should be directed to and will be fulfilled by the Lead Contact, Zhiyong Ma (mazhy@mail.buct.edu.cn).

Materials Availability

All materials generated in this study will be made available on reasonable request.

Syntheses of CNPyBCz and CNBrBCz

Potassium tert-butoxide (1.3465 g, 12 mmol), BCz-2 (1.0033 g, 6 mmol) and 3-Cyano-2-fluoropyridine (0.7055 g, 5 mmol) were added to a 100 mL shrek bottle. Then sealing the bottle and fill it with nitrogen. DMF (10 mL, AR grade) was add to the bottle and the mixed solution was refluxed at 110 ℃ for 24h in nitrogen atmosphere. After the reaction was over, the resultant mixture was cooled down to room temperature and the solvent was washed by deionized water and ethyl acetate. Yield: 99%. Following the similar synthesis of CNPyBCz, CNBrBCz was obtained as white powder by using 3-Bromo-5-fluorobenzonitrile in place of 2-Cyano-3-fluoropyridine. Yield: 60%.

Materials Characterization

^{1}H NMR was recorded on the 400 MHz (Bruker ARX400) and ^{13}C NMR spectra were recorded on the Bruker 101 MHz spectrometer at room temperature with $CDCl_3$, DMSO-d_6 and *d*-DMF as the solvents and tetramethylsilane (TMS) as the internal standard. ESI high resolution mass-spectra (HRMS) were acquired on a Waters Xevo G2 Qt of mass spectrometer. Transient and delayed photoluminescence spectra were performed on the Hitachi F-4600 or Edinburgh Instruments FLS980 fluorescence spectrophotometer. Luminescence lifetime were acquired on the Edinburgh Instruments FLS980 fluorescence spectrophotometer or Deltaflex Fluorescence Lifetime Instrument (λ_{ex}=365 nm). Single crystal X-ray diffraction data were collected with a NONIUS KappaCCD diffractometer with graphite monochromator and Mo Kα radiation [λ (MoKα) = 0.71073 Å]. Structures were solved by direct methods with SHELXS-97 and refined against F2 with SHELXS-97.

ACKNOWLEDGMENTS

This work is financially supported by the National Natural Science Foundation of China (22175015, 22174002), the Beijing Natural Science Foundation (2182054), the Big

Science Project from BUCT (XK180301), and the Fundamental Research Funds for the Central Universities to Z. Y. Ma.

Author contributions

Xiaohua Fu and Xue Zhang contributed equally to this work.

Declaration of interests

The authors declare no competing interests.

References

1. Ma, X., Xu, C., Wang, J., and Tian, H. (2018). Amorphous Pure Organic Polymers for Heavy-Atom-Free Efficient Room-Temperature Phosphorescence Emission. Angew. Chem. Int. Ed. *57*, 10854-10858.
2. Yanxiang, G., Jie, Y., Manman, F., and Zhen, L. (2021). Room-temperature phosphorescence from metal-free polymer-based materials. Cell Rep. Phys. Sci. *3*, 100663.
3. Forni, A., Lucenti, E., Botta, C., and Cariati, E. (2018). Metal free room temperature phosphorescence from molecular self-interactions in the solid state. J. Mater. Chem. C 6, 4603-4626.
4. Feng, Q., Xie, Z., and Zheng, M. (2020). Colour-Tunable Ultralong-Lifetime Room Temperature Phosphorescence with External Heavy-Atom Effect in Boron-Doped Carbon Dots. Chem. Eng. J. 420, 127647.
5. Liu, Y., Ma, Z., Liu, J., Chen, M., Ma, Z., and Jia, X. (2021). Robust White-Light Emitting and Multi-Responsive Luminescence of a Dual-Mode Phosphorescence Molecule. Adv. Opt. Mater. 9, 2001685.
6. Mane, S.K.B., Mu, Y., Ubba, E., Yang, Z., Zhao, J., and Chi, Z. (2019). Tuning the organic persistent room-temperature phosphorescence through aggregated states†. J. Mater. Chem. C 7, 15219-15224.
7. Li, D., Yang, Y., Yang, J., Fang, M., Tang, B.Z., and Li, Z. (2022). Completely aqueous processable stimulus responsive organic room temperature phosphorescence materials with tunable afterglow color. Nat. Commun. 13, 347.
8. Gu, L., Shi, H., Bian, L., Gu, M., Ling, K., Wang, X., Ma, H., Cai, S., Ning, W., Fu, L., et al. (2019). Colour-tunable ultra-long organic phosphorescence of a single-component molecular crystal. Nat. Photonics 13, 406-411.
9. Xiang, H., Cheng, J., Ma, X., Zhou, X., and Chruma, J.J. (2013). Near-infrared phosphorescence: materials and applications. Chem. Soc. Rev. 42, 6128-6185.
10. Fateminia, S.M.A., Mao, Z., Xu, S., Yang, Z., Chi, Z., and Liu, B. (2017). Organic Nanocrystals with Bright Red Persistent Room-Temperature Phosphorescence for Biological Applications. Angew. Chem. Int. Ed. 56, 12160-12164.
11. Wang, Y., Gao, H., Yang, J., Fang, M., Ding, D., Tang, B.Z., and Li, Z. (2021). High Performance of Simple Organic Phosphorescence Host–Guest Materials and their Application in Time-Resolved Bioimaging. Adv. Mater. 33, 2007811.
12. Yang, J., Gao, H., Wang, Y., Yu, Y., Gong, Y., Fang, M., Ding, D., Hu, W., Tang, B.Z., and Li, Z. (2019). The odd–even effect of alkyl chain in organic room temperature phosphorescence luminogens and the corresponding in vivo imaging†. Mater. Chem. Front. 3, 1391-1397.
13. Ding, Y., Wang, X., Tang, M., and Qiu, H. (2021). Tailored Fabrication of Carbon Dot Composites with

Full-Color Ultralong Room-Temperature Phosphorescence for Multidimensional Encryption. Adv. Sci. 9, e2103833.

14. Tan, J., Li, Q., Meng, S., Li, Y., Yang, J., Ye, Y., Tang, Z., Qu, S., and Ren, X. (2021). Time-Dependent Phosphorescence Colors from Carbon Dots for Advanced Dynamic Information Encryption. Adv. Mater. 33, e2006781.
15. Lin, C., Zhuang, Y., Li, W., Zhou, T.-L., and Xie, R.-J. (2018). Blue, green, and red full-color ultralong afterglow in nitrogen-doped carbon dots†. Nanoscale 11, 6584-6590.
16. Liu, Y., Al-salihi, M., Guo, Y., Ziniuk, R., Cai, S., Wang, L., Li, Y., Yang, Z., Peng, D., Xi, K., et al. (2022). Halogen-doped phosphorescent carbon dots for grayscale patterning. Light Sci. Appl. 11, 163.
17. Xueqiang, C., Wenbo, D., Xinghui, W., Han, S., Cong, C., Yunxiang, L., Jianbing, S., Bin, T., Zhengxu, C., and Yuping, D. (2021). Fluorene-based host-guest phosphorescence materials for information encryption. Chem. Eng. J. 426, 131607.
18. Li, Q., and Li, Z. (2017). The Strong Light-Emission Materials in the Aggregated State: What Happens from a Single Molecule to the Collective Group. Adv. Sci. 4, 1600484.
19. Huang, L., Liu, L., Li, X., Hu, H., Chen, M., Yang, Q., Ma, Z., and Jia, X. (2019). Crystal-State Photochromism and Dual-Mode Mechanochromism of an Organic Molecule with Fluorescence, Room-Temperature Phosphorescence, and Delayed Fluorescence. Angew. Chem. Int. Ed. 58, 16445-16450.
20. Green, D.C., Holden, M.A., Levenstein, M.A., Zhang, S., Johnson, B.R.G., Gala de Pablo, J., Ward, A., Botchway, S.W., and Meldrum, F.C. (2019). Controlling the fluorescence and room-temperature phosphorescence behaviour of carbon nanodots with inorganic crystalline nanocomposites. Nat. Commun. 10, 206.
21. Xiao, F., Gao, H., Lei, Y., Dai, W., Liu, M., Zheng, X., Cai, Z., Huang, X., Wu, H., and Ding, D. (2022). Guest-host doped strategy for constructing ultralong-lifetime near-infrared organic phosphorescence materials for bioimaging. Nat. Commun. 13, 186.
22. Nannan, L., Yanyan, P., Yunxiang, L., Miaochang, L., Chengdong, P., Zhengxu, C., Guomin, S., Huayue, W., Xiaobo, H., and Yuping, D. (2021). Protic Acids as Third Components Improve the Phosphorescence Properties of the Guest-Host System Through Hydrogen Bonds. Chem. Eng. J. 433, 133530.
23. Chong, K.C., Chen, C., Zhou, C., Chen, X., Ma, D., Bazan, G.C., Chi, Z., and Liu, B. (2022). Structurally Resemblant Dopants Enhance Organic Room-Temperature Phosphorescence. Adv. Mater. 34, e2201569.
24. Zhang, X., Du, L., Zhao, W., Zhao, Z., Xiong, Y., He, X., Gao, P.F., Alam, P., Wang, C., Li, Z., et al. (2019). Ultralong UV/mechano-excited room temperature phosphorescence from purely organic cluster excitons. Nat. Commun. 10, 5161.
25. Jiayao, S., Chen, Q., Zhimin, M., Shitao, W., and Zhiyong, M. (2022). A host-guest organic afterglow system with significant guest induced enhancement of phosphorescence. Dyes Pigm. 201, 110196.
26. Chen, C., Chi, Z., Chong, K.C., Batsanov, A.S., Yang, Z., Mao, Z., Yang, Z., and Liu, B. (2021). Carbazole isomers induce ultralong organic phosphorescence. Nat. Mater. 20, 175-180.
27. Qian, C., Ma, Z., Yang, B., Li, X., Sun, J., Li, Z., Jiang, H., Chen, M., Jia, X., and Ma, Z. (2021). Carbazole&benzoindole-based purely organic phosphors: a comprehensive phosphorescence mechanism, tunable lifetime and an advanced encryption system. J. Mater. Chem. C 9, 14294-14302.
28. Chen, C., Chong, K.C., Pan, Y., Qi, G., Xu, S., and Liu, B. (2021). Revisiting Carbazole: Origin, Impurity, and Properties. ACS Mater. Lett. 3, 1081-1087.
29. Qian, C., Ma, Z., Fu, X., Zhang, X., Li, Z., Jin, H., Chen, M., Jiang, H., Jia, X., and Ma, Z. (2022). More than Carbazole Derivatives Activate Room Temperature Ultralong Organic Phosphorescence of Benzoindole Derivatives. Adv. Mater. 34, 2200544.

30. Garain, S., Sarkar, S., Chandra Garain, B., Pati, S.K., and George, S.J. (2022). Chiral Arylene Diimide Phosphors: Circularly Polarized Ambient Phosphorescence from Bischromophoric Pyromellitic Diimides. Angew. Chem. Int. Ed. 61, e202115773.
31. Yang, Y., Liang, Y., Zheng, Y., Li, J.-A., Wu, S., Zhang, H., Huang, T., Luo, S., Liu, C., Shi, G., et al. (2022). Efficient and Color-Tunable Dual-Mode Afterglow from Large-Area and Flexible Polymer-Based Transparent Films for Anti-Counterfeiting and Information Encryption. Angew. Chem. Int. Ed. 61, e202201820.
32. Zhang, J.-C., Pan, C., Zhu, Y.-F., Zhao, L.-Z., He, H.-W., Liu, X., and Qiu, J. (2018). Achieving Thermo-Mechano-Opto-Responsive Bitemporal Colorful Luminescence via Multiplexing of Dual Lanthanides in Piezoelectric Particles and its Multidimensional Anticounterfeiting. Adv. Mater. 30, e1804644.
33. Zhang, Y., Gao, L., Zheng, X., Wang, Z., Yang, C., Tang, H., Qu, L., Li, Y., and Zhao, Y. (2021). Ultraviolet irradiation-responsive dynamic ultralong organic phosphorescence in polymeric systems. Nat. Commun. 12, 2297.
34. Wang, S., Xu, M., Huang, K., Zhi, J., Sun, C., Wang, K., Zhou, Q., Gao, L., Jia, Q., Shi, H., et al. (2019). Biocompatible metal-free organic phosphorescent nanoparticles for efficiently multidrug-resistant bacteria eradication. Sci. China Mater. 63, 316-324.
35. Xu, Z., Jiang, Y., Shen, Y., Tang, L., Hu, Z., Lin, G., Law, W.-C., Ma, M., Dong, B., Yong, K.-T., et al. (2022). A biocompatible photosensitizer with a high intersystem crossing efficiency for precise two-photon photodynamic therapy. Mater. Horiz. 9, 1283-1292.
36. Xiong, Y., Zhao, Z., Zhao, W., Ma, H., Peng, Q., He, Z., Zhang, X., Chen, Y., He, X., Lam, J.W.Y., et al. (2018). Designing Efficient and Ultralong Pure Organic Room-Temperature Phosphorescent Materials by Structural Isomerism. Angew. Chem. Int. Ed. 57, 7997-8001.
37. Cheng, A., Jiang, Y., Su, H., Zhang, B., Jiang, J., Wang, T., Luo, Y., and Zhang, G. (2022). Origin of Red-Shifted Phosphorescence from Triphenylamines: Triplet Excimer or Impurity? Angew. Chem. Int. Ed. 61, e202206366.
38. Chen, B., Huang, W., Nie, X., Liao, F., Miao, H., Zhang, X., and Zhang, G. (2021). An Organic Host–Guest System Producing Room-Temperature Phosphorescence at the Parts-Per-Billion Level. Angew. Chem. Int. Ed. 60, 16970-16973.
39. An, Z., Zheng, C., Tao, Y., Chen, R., Shi, H., Chen, T., Wang, Z., Li, H., Deng, R., Liu, X., et al. (2015). Stabilizing triplet excited states for ultralong organic phosphorescence. Nat. Mater. 14, 685-690.
40. Cai, S., Shi, H., Li, J., Gu, L., Ni, Y., Cheng, Z., Wang, S., Xiong, W.-w., Li, L., An, Z., et al. (2017). Visible-Light-Excited Ultralong Organic Phosphorescence by Manipulating Intermolecular Interactions. Adv. Mater. 29, 1701244.
41. Xie, Y., Ge, Y., Peng, Q., Li, C., Li, Q., and Li, Z. (2017). How the Molecular Packing Affects the Room Temperature Phosphorescence in Pure Organic Compounds: Ingenious Molecular Design, Detailed Crystal Analysis, and Rational Theoretical Calculations. Adv. Mater. 29, 1606829.
42. Kenry, Chen, C., and Liu, B. (2019). Enhancing the performance of pure organic room-temperature phosphorescent luminophores. Nat. Commun. 10, 2111.
43. Huang, L., Qian, C., and Ma, Z. (2020). Stimuli-Responsive Purely Organic Room-Temperature Phosphorescence Materials. Chemistry – A European Journal 26, 11914-11930.
44. Chen, J., Chen, X., Cao, L., Deng, H., Chi, Z., and Liu, B. (2022). Synergistic Generation and Accumulation of Triplet Excitons for Efficient Ultralong Organic Phosphorescence. Angew. Chem. Int. Ed. 61, e202200343.
45. Zhang, Q., Fan, Y., Liao, Q., Zhong, C., Li, Q., and Li, Z. (2022). Room temperature phosphorescence achieved by aromatic/perfluoroaromatic interactions. Sci. China Chem. 65, 918-925.
46. Jinnai, K., Kabe, R., Lin, Z., and Adachi, C. (2022). Organic long-persistent luminescence stimulated by

visible light in p-type systems based on organic photoredox catalyst dopants. Nat. Mater. 21, 338-344.

47. Kabe, R., and Adachi, C. (2017). Organic long persistent luminescence. Nature 550, 384-387.
48. Yamanaka, T., Nakanotani, H., and Adachi, C. (2019). Slow recombination of spontaneously dissociated organic fluorophore excitons. Nat. Commun. 10, 5748.
49. Yamanaka, T., Nakanotani, H., and Adachi, C. (2022). Significant role of spin-triplet state for exciton dissociation in organic solids. Sci. Adv. 8, eabj9188.